主論文
平成25年9月発行　Medical Physics
第40巻　第9号　091705-1～091705-8

Predictive uncertainty in infrared marker-based dynamic tumor tracking with Vero4DRT

Mami Akimoto[1], Mitsuhiro Nakamura*[1], Nobutaka Mukumoto[1], Hiroaki Tanabe[2], Masahiro Yamada[1], Yukinori Matsuo[1], Hajime Monzen[1], Takashi Mizowaki[1], Masaki Kokubo[2,3], and Masahiro Hiraoka[1]

1. Department of Radiation Oncology and Image-applied Therapy, Graduate School of Medicine, Kyoto University, Kyoto 606-8507, Japan
2. Division of Radiation Oncology, Institute of Biomedical Research and Innovation, Hyogo 650-0047, Japan
3. Department of Radiation Oncology, Kobe City Medical Center General Hospital, Hyogo 650-0047, Japan

***Corresponding author**: Mitsuhiro Nakamura, P_H.D., Graduate School of Medicine, Kyoto University, 54 Kawahara-cho, Shogoin, Sakyo-ku, Kyoto, Kyoto 606-8507, Japan.
Tel.: +81-75-751-3762; Fax: +81-75-771-9749; E-mail: m_nkmr@kuhp.kyoto-u.ac.jp

Running title: Predictive uncertainty in IR Tracking

Conflicts of interest: This research was sponsored in part by Mitsubishi Heavy Industries, Ltd., Japan. Takashi Mizowaki, Masaki Kokubo, and Masahiro Hiraoka have consultancy agreement with Mitsubishi Heavy Industries, Ltd., Japan.

Meeting presentation: This work will be presented in part at the oral session of the 2nd ESTRO Forum in Geneva, April 19–23, 2013.

Abstract

Purpose: To quantify the predictive uncertainty in infrared (IR)-marker-based dynamic tumor tracking irradiation (IR Tracking) with Vero4DRT (MHI-TM2000) for lung cancer using logfiles.

Methods: A total of 110 logfiles for 10 patients with lung cancer who underwent IR Tracking were analyzed. Before beam delivery, external IR markers and implanted gold markers were monitored for 40 s with the IR camera every 16.7 ms and with an orthogonal kV x-ray imaging subsystem every 80 or 160 ms. A predictive model [four-dimensional (4D) model] was then created to correlate the positions of the IR markers (P_{IR}) with the three-dimensional (3D) positions of the tumor indicated by the implanted gold markers (P_{detect}). The sequence of these processes was defined as 4D modeling. During beam delivery, the 4D model predicted the future 3D target positions ($P_{predict}$) from the P_{IR} in real-time, and the gimbaled x-ray head then tracked the target continuously. In clinical practice, we updated the 4D model at least once during each treatment session to improve its predictive accuracy. This study evaluated the predictive errors in 4D modeling (E_{4DM}) and those resulting from the baseline drift of P_{IR} and P_{detect} during a treatment session (E_{BD}). E_{4DM} was defined as the difference between $P_{predict}$ and P_{detect} in 4D modeling, and E_{BD} was defined as the mean difference between $P_{predict}$ calculated from P_{IR} in updated 4D modeling using (a) a 4D model created from training data before the model update and (b) an updated 4D model created from new training data.

Results: The mean E_{4DM} was 0.0 mm with the exception of one logfile. Standard deviations of E_{4DM} ranged from 0.1–1.0, 0.1–1.6, and 0.2–1.3 mm in the left-right (LR), anterior-posterior (AP), and superior-inferior (SI) directions, respectively. The median

elapsed time before updating the 4D model was 13 (range, 2–33) min, and the median frequency of 4D modeling was twice (range, 2–3 times) per treatment session. E_{BD} ranged from -1.0–1.0, -2.1–3.3, and -2.0–3.5 mm in the LR, AP, and SI directions, respectively. E_{BD} was highly correlated with BD_{detect} in the LR (R=-0.83) and AP directions (R=-0.88), but not in the SI direction (R=-0.40). Meanwhile, E_{BD} was highly correlated with BD_{IR} in the SI direction (R=-0.67), but not in the LR (R=0.15) or AP (R=-0.11) direction. If the 4D model was not updated in the presence of intrafractional baseline drift, the predicted target position deviated from the detected target position systematically.

Conclusions: Application of IR Tracking substantially reduced the geometric error caused by respiratory motion; however, an intrafractional error due to baseline drift of >3 mm was occasionally observed. To compensate for E_{BD}, we recommend checking the target and IR marker positions constantly and updating the 4D model several times during a treatment session.

Key words: Motion management, Predictive uncertainty, IR Tracking, Respiratory surrogates, Vero4DRT.

I. INTRODUCTION

The management of respiratory motion is one of the most important issues in high-precision radiotherapy.[1,2] Without managing respiratory motion, normal tissues surrounding the target will receive an unnecessary dose, which might increase the rate of normal tissue complications. A variety of methods have been proposed to reduce the impact of respiratory motion during beam delivery, including motion-encompassing, forced shallow-breathing, breath hold, respiratory gated, and dynamic tumor tracking (DTT) methods.[2]

Of these methods, recent interest has focused on the DTT technique, which can reposition the radiation beam dynamically in accordance with the target position. DTT methods are categorized as direct and indirect.[3] Direct methods detect the internal target itself or surrogates within or near the target using imaging modalities. Indirect DTT methods observe external surrogates and then deduce the internal target position from the surrogates.

The CyberKnife Robotic Radiosurgery System with the integrated Synchrony Respiratory Tracking System (Accuray, Sunnyvale, CA) was the first clinically available radiotherapy unit to realize indirect DTT irradiation.[4] The Synchrony system compensates for tumor motion by moving the robotic arm based on the target position predicted from the motion of light-emitting diodes on the chest, which can substantially reduce the geometric error caused by respiratory motion;[5-7] however, several researchers reported that the correlation between internal target positions and external surrogates can change in the presence of phase shift and inter- and intrafractional baseline drift, reducing the accuracy of the correlation model.[5,7]

Vero4DRT [MHI-TM2000; Mitsubishi Heavy Industries (MHI), Ltd., Japan,

and BrainLAB, Feldkirchen, Germany] is an innovative radiotherapy unit with an integrated DTT system. Vero4DRT has an orthogonal kV x-ray imaging subsystem comprising two sets of x-ray tubes and flat-panel detectors with a spatial resolution of 0.2 mm at the isocenter level and a gimbaled x-ray head with a compact 6-MV C-band linac in an O-shaped gantry (O-ring), which provides real-time imaging and tumor motion compensation.[8,9] With these features, Vero4DRT is capable of both direct and indirect DTT.[10,11] At present, an infrared (IR)-marker-based DTT (IR Tracking), which is categorized as an indirect DTT method, is available clinically. The IR Tracking system predicts the future target position from the positions of IR markers on the abdominal wall using a predictive model [four-dimensional (4D) model]. We have applied IR Tracking clinically to lung cancer patients since September 2011.[12]

A key issue in IR Tracking is the accuracy of the 4D model in terms of predicting the internal target position from the surrogate measurements. Here, we assessed the predictive uncertainty relevant to the 4D model in IR Tracking.

II. MATERIALS AND METHODS

II.A. Patients

This study included 10 lung cancer patients [eight males, two females; median age 84 (range, 60–87) years] who underwent IR Tracking. Their lung tumors were located in the right middle (one patient), right lower (six patients) and left lower (three patients) lobes. The patients were treated with 6–8 non-coplanar beams. The prescribed dose was 48 or 56 Gy in four fractions at the isocenter. Four or five 1.5-mm-diameter gold markers were implanted around the lung tumor transbronchially 1–2 weeks before

120 treatment planning. All patients were fixed in the supine position on an individualized
121 vacuum pillow with both arms raised.
122
123 **II.B. Procedure of IR Tracking**
124 Figure 1 shows a schematic diagram of the IR Tracking procedure. First, the
125 setup error was corrected based on the bony anatomy. The IR and implanted gold
126 markers were then monitored synchronously for 40 s with an IR camera on the ceiling
127 of the treatment room every 16.7 ms and with the orthogonal kV x-ray imaging
128 subsystem every 80 or 160 ms. The sampling time of the kV x-ray images automatically
129 changed to 160 ms when the velocity of the IR marker motion decreased. The attitude of
130 the O-ring used for monitoring the implanted gold markers was determined with
131 reference to our previous study.[13] The positions of gold markers were detected
132 automatically using the intensity ratio of the gold marker to its surroundings.[13] Using
133 these training data, a 4D model was created to correlate the 3D target positions
134 indicated by the implanted gold markers (detected target positions, P_{detect}) with the IR
135 marker positions on the abdominal wall (P_{IR}). The 4D model was expressed as follows:
136 $$P_{predict}=aP_{IR}^2+bP_{IR}+c+dv_{IR}^2+ev_{IR},$$
137 where $P_{predict}$ is the predicted target position and v_{IR} is the vertical velocity of the IR
138 markers. The sequence of these processes was defined as 4D modeling in the current
139 study. Details of determination of each parameter are described in Section II.C. During
140 beam delivery, the IR Tracking system anticipates the $P_{predict}$ from P_{IR} using the 4D
141 model parameters in real time, and the gimbaled head then tracks the moving target
142 continuously. In clinical practice, we monitored the implanted gold markers on
143 orthogonal kV x-ray images during beam delivery. The predicted positions with

144 arbitrary radius circles around the implanted gold markers (tolerance circles; green
145 circles in Fig. 2) were displayed as a benchmark of the 4D model update. The 4D model
146 update was needed when the implanted gold markers deviated systematically from the
147 tolerance circles. In the current study, the 4D model update was performed at least once
148 during each treatment session to improve the predictive accuracy.

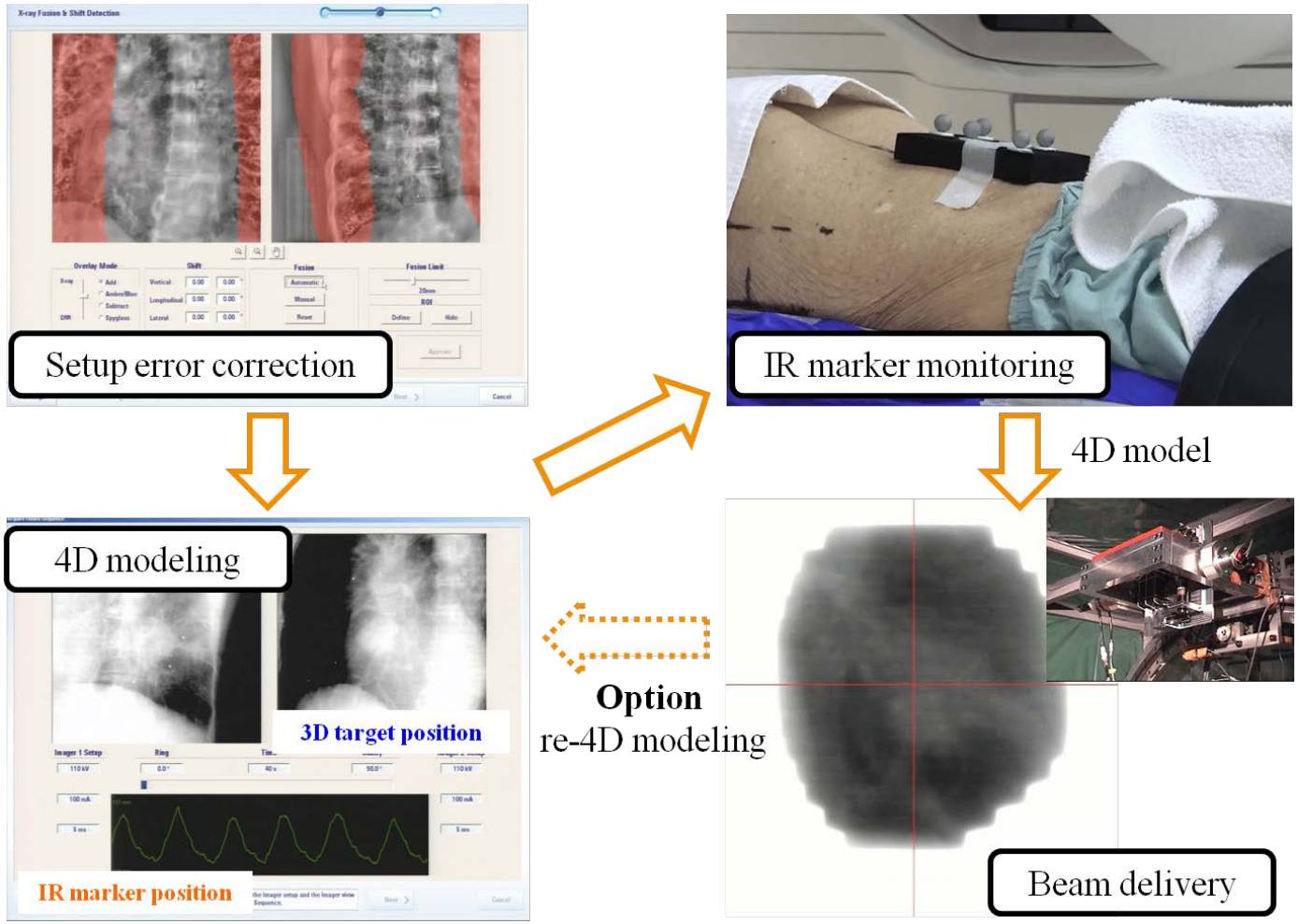

Figure 1. A schematic diagram of the IR Tracking procedure using the Vero4DRT system.

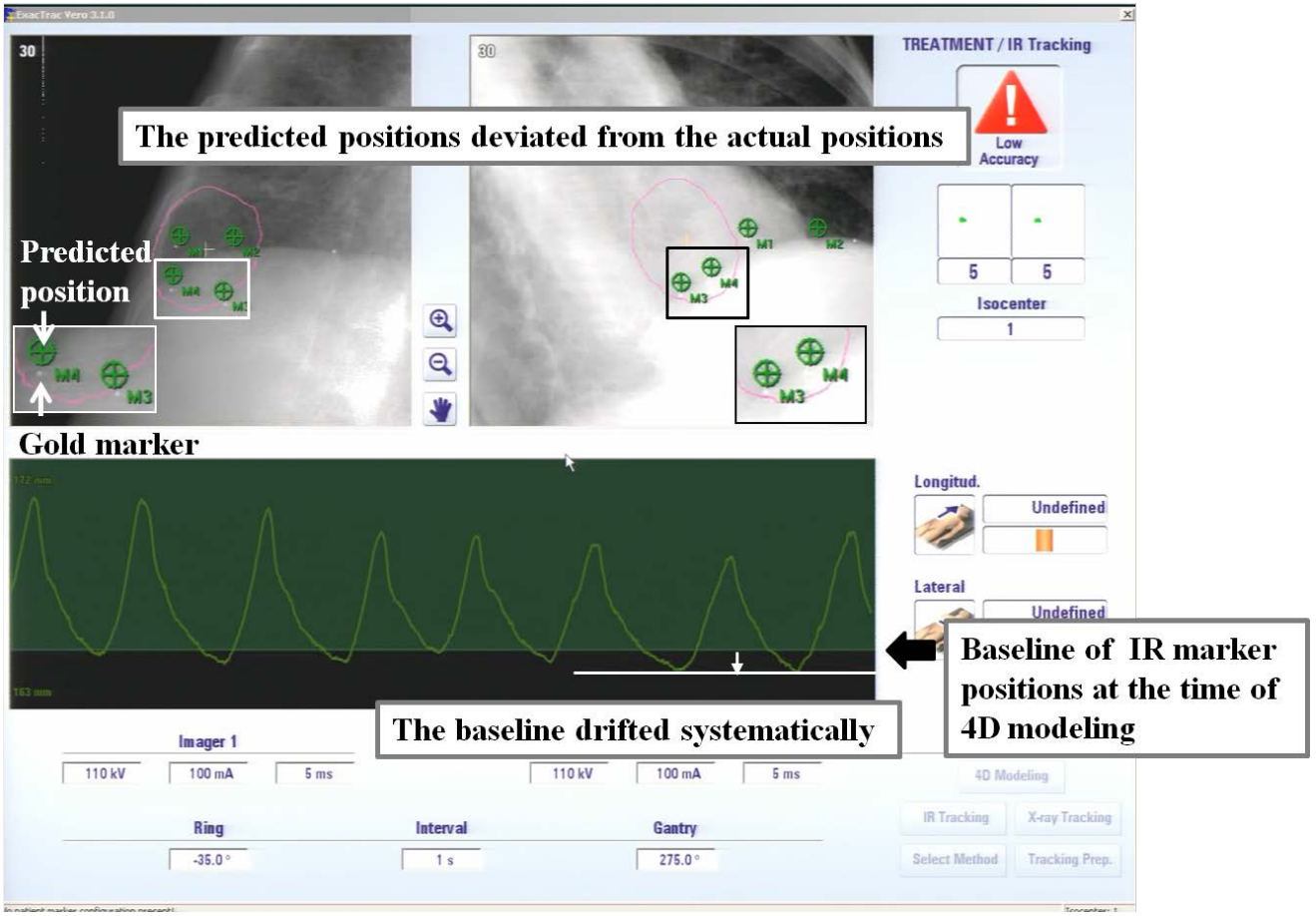

Figure 2. A screenshot during IR Tracking irradiation in a case of large baseline drift of the IR marker positions. When the predicted target positions deviated from the internal gold markers systematically, additional 4D modeling was performed.

II.C. Calculation of predicted target positions

Based on available information from the vendor, the predicted target position was calculated from P_{IR} and P_{detect} as follows;

(1) Prediction of the IR marker position after 25 ms: Using the previous multiple consecutive positions of the k^{th} IR marker ($P_{IR,k}$; $1 \leq k \leq 5$) before time t, the P_{IR} after 25 ms [$P_{IR,k}'(t+25)$] was predicted using a linear approximate equation that was determined using the weighted least-squares method. A time interval of 25 ms was required to compensate for the system latency of IR Tracking, which was disclosed by MHI.

(2) Calculation of the velocity of IR marker motion: The velocity at time t+25 ms [$v_{IR,k}'(t+25)$] was calculated from $P_{IR,k}$ and $P_{IR,k}'$, assuming that the velocity was constant at t+25 ms.

(3) Association of 3D target position with IR marker position and velocity: Using multiple regression analysis, 4D model parameters (a_k, b_k, c_k, d_k, and e_k) were determined by minimizing the residual errors between P_{detect} and the target positions predicted from the displacement of the k^{th} IR marker using the above equation in Section II.B.

(4) Calculation of 3D target position based on multiple IR markers: Processes (1) to (3) were repeated for each IR marker, and the predicted target position for the k^{th} IR marker ($P_{predict,k}$) was then calculated from the displacement of the k^{th} IR marker using the determined 4D model parameters. The mean of $P_{predict,k}$ was regarded as $P_{predict}$.

II.D. Data analysis

178 The logfiles of 4D models containing P_{IR}, $P_{predict}$, and P_{detect} were used for the
179 data analysis. The metrics for assessing them and their definitions were as follows:
180 (1) Motion amplitude of the detected target positions (A): Median peak-to-peak
181 amplitude of P_{detect}.
182 (2) Baseline drift of the IR marker (BD_{IR}) and detected target (BD_{detect}) positions:
183 The difference in the baselines of P_{IR} and P_{detect} between the last 4D modeling
184 before re-4D modeling [$(n\text{-}1)^{th}$ 4D modeling] and re-4D modeling (n^{th} 4D
185 modeling). The baselines were defined as the median position among the peaks
186 of P_{IR} and P_{detect} at the end-expiration phase during the 4D modeling. Positive
187 values of BD_{IR} indicate an anterior direction and those of BD_{detect} indicate left,
188 anterior, and inferior directions.
189 (3) Absolute correlation coefficient between internal and external respiratory
190 signals ($|R_{IR}^{target}|$): Absolute correlation coefficient between P_{detect} and P_{IR}.
191 (4) 4D modeling errors (E_{4DM}): The predictive errors in 4D modeling. E_{4DM} was
192 defined as the difference between P_{detect} and $P_{predict}$ in 4D modeling (Fig. 3).
193 (5) Intrafractional errors due to baseline drift (E_{BD}): The predictive errors resulting
194 from BD_{IR} and BD_{detect} during a treatment session. E_{BD} was defined as the mean
195 difference between $P_{predict}$ calculated from P_{IR} in the updated 4D modeling
196 using (a) a 4D model created from training data before the model update
197 [$(n\text{-}1)^{th}$ 4D model], and (b) an updated 4D model created from the new training
198 data (n^{th} 4D model) (n=2–3) (Fig. 3).

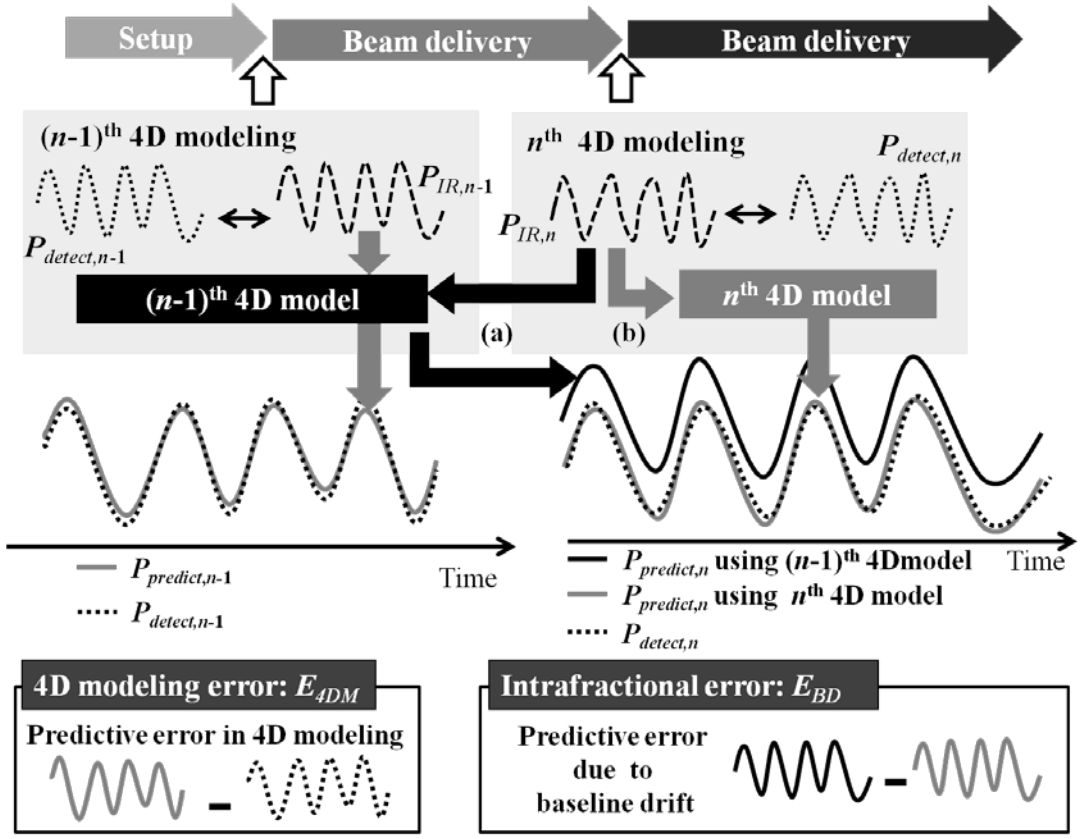

Figure 3. A schematic diagram for calculating 4D modeling errors (E_{4DM}) and intrafractional errors due to baseline drift (E_{BD}). E_{4DM} was defined as the difference between P_{detect} and $P_{predict}$ in 4D modeling. E_{BD} was defined as the mean difference between $P_{predict}$ calculated from P_{IR} in n^{th} 4D modeling using (a) a $(n\text{-}1)^{th}$ 4D model, and (b) a n^{th} 4D model.

In total, 110 logfiles were analyzed to assess the predictive uncertainties in IR Tracking. For BD_{IR}, BD_{detect}, and E_{BD}, a dataset of 53 paired logfiles was analyzed.

III. RESULTS

III.A. Motion amplitude and baseline drift

The median A was 1.4 (range, 0.2–5.6), 3.0 (range, 0.9–6.6), and 11.0 (range, 1.4–23.5) mm in the left-right (LR), anterior-posterior (AP), and superior-inferior (SI) directions, respectively.

The median elapsed time before updating the 4D model was 13 (range, 2–33) min, and the median frequency of 4D modeling was twice (range, 2–3 times) per treatment session. The median BD_{IR} was -0.3 (range, -3.2–1.3) mm. The baseline of the IR markers drifted mainly in the posterior direction for 39 paired logfiles (74%). The median BD_{detect} was 0.0 (range, -1.2–0.9), -0.4 (range, -3.6–1.8), and 0.2 (range, -1.6–5.0) mm in the LR, AP, and SI directions, respectively. BD_{detect} drifted in the posterior and superior directions for 38 (72%) and 35 (66%) paired logfiles, respectively. There were no significant correlations between BD_{IR} and BD_{detect} in the LR (R=-0.01), AP (R=0.40), and SI directions (R=-0.30).

III.B. Correlation between internal and external respiratory signals and 4D modeling errors

The median $|R_{IR}^{target}|$ was 0.76 (range, 0.03–0.98), 0.80 (range, 0.01–0.97), and 0.98 (range, 0.15–1.00) in the LR, AP, and SI directions, respectively. $|R_{IR}^{target}| > 0.7$, which indicates high correlation,[14] was observed for 63 (57.3%), 65 (59.1%), and

100 (91.0%) logfiles in the LR, AP, and SI directions, respectively. Meanwhile, $|R_{IR}^{target}| < 0.2$, which indicates poor correlation,[14] was observed for seven (6.4%), eight (7.3%), and two (1.8%) logfiles in the LR, AP, and SI directions, respectively.

Excluding the case in which the mean E_{4DM} was -0.1 mm in the AP direction for one logfile (0.9%), the mean E_{4DM} was 0.0 mm for all remaining logfiles. The SD of E_{4DM} ranged from 0.1–1.0, 0.1–1.6, and 0.2–1.3 mm in the LR, AP, and SI directions, respectively.

III.C. Intrafractional errors due to baseline drift

E_{BD} ranged from -1.0–1.0, -2.1–3.3, and -2.0–3.5 mm in the LR, AP, and SI directions, respectively. Figure 4(a) shows P_{IR} and its baseline during the $(n\text{-}1)^{th}$ and n^{th} 4D modeling, and Fig. 4(b) shows P_{detect} and $P_{predict}$ calculated from P_{IR} in the n^{th} 4D modeling using $(n\text{-}1)^{th}$ and n^{th} 4D models in Patient 2, who had the largest E_{BD}. As shown in Fig. 4(b), $P_{predict}$ deviated from P_{detect} systematically if the 4D model was not updated in the presence of intrafractional baseline drift.

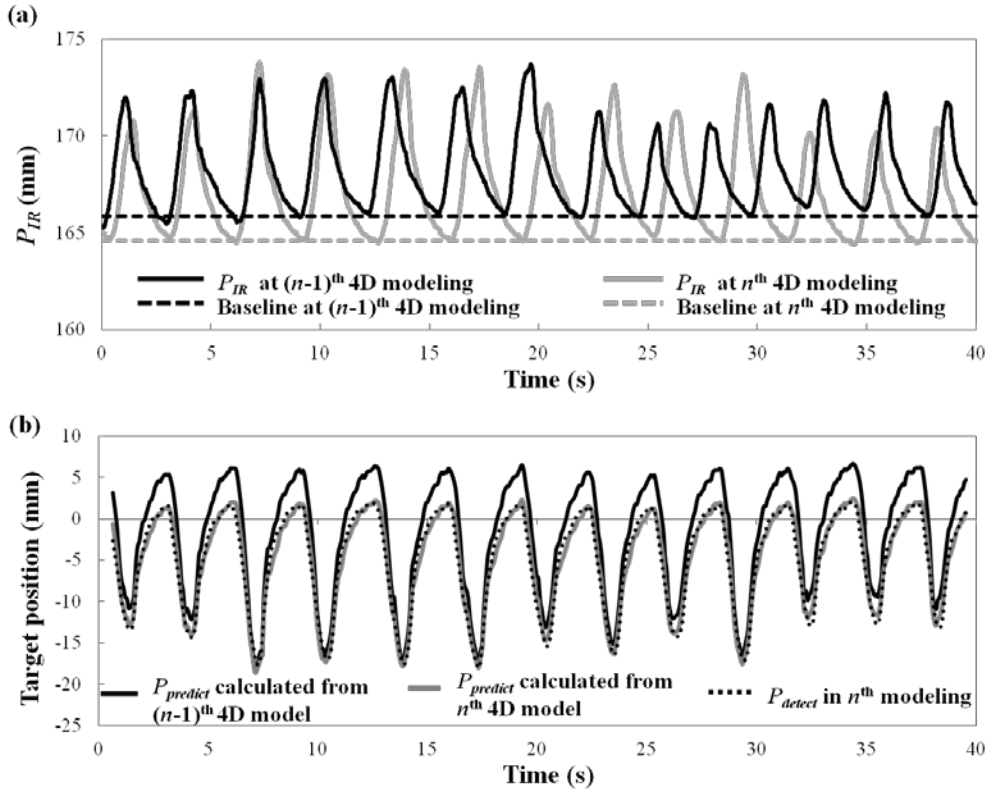

Figure 4. (a) The IR marker positions (P_{IR}; solid curve) and their baselines (dotted curve) during the $(n\text{-}1)^{th}$ (black curve) and n^{th} 4D modeling (gray curve), and (b) the predicted target positions ($P_{predict}$) calculated from P_{IR} in the n^{th} 4D modeling using the $(n\text{-}1)^{th}$ (black curve) and n^{th} 4D models (gray curve) and the detected target positions in n^{th} 4D modeling (P_{detect}; dotted curve) for Patient 2, who had the largest E_{BD}.

247 Figure 5 shows E_{BD} as a function of BD_{detect}. E_{BD} was highly correlated with
248 BD_{detect} in the LR (R=-0.83) and AP directions (R=-0.88), but not in the SI direction
249 (R=-0.40). While BD_{detect} in the LR direction was within 2 mm for all paired logfiles,
250 BD_{detect} > 2 mm was observed in three paired logfiles (6%) in the AP direction and in
251 five paired logfiles (9%) in the SI direction. This large BD_{detect} was observed mainly in
252 Patient 6.

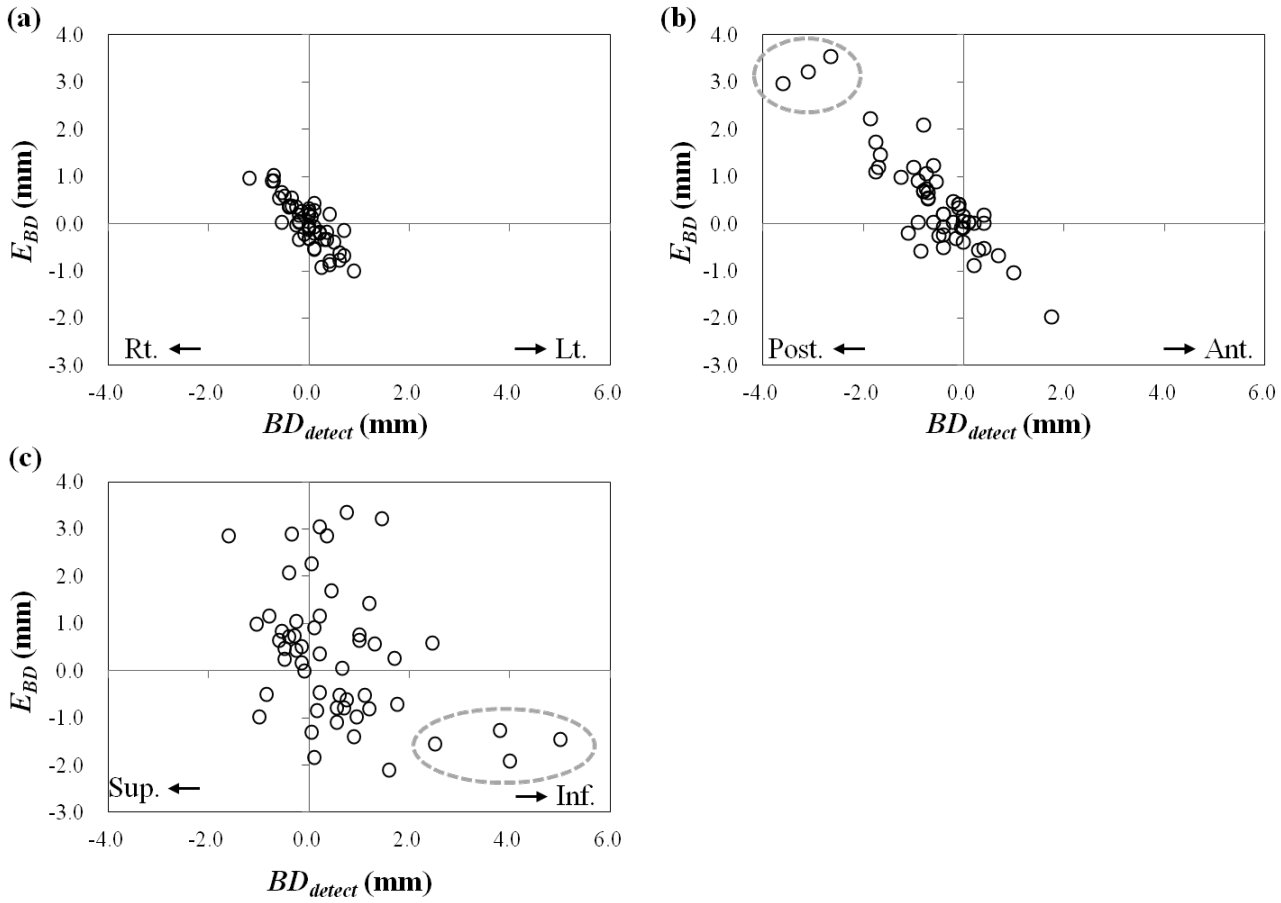

253

254 **Figure 5.** E_{BD} as a function of the baseline drift of the detected target positions (BD_{detect}) in the (a) LR, (b) AP, and (c) SI directions.

255 $|BD_{detect}| > 2$ mm in Patient 6 is surrounded by a gray dotted ellipse.

256 Figure 6 shows E_{BD} as a function of BD_{IR}. Excluding the case in which BD_{detect}
257 was >2 mm in Patient 6 (triangles), E_{BD} was highly correlated with BD_{IR} in the SI
258 direction (R=-0.67), but not in the LR (R=0.15) or AP (R=-0.11) direction.

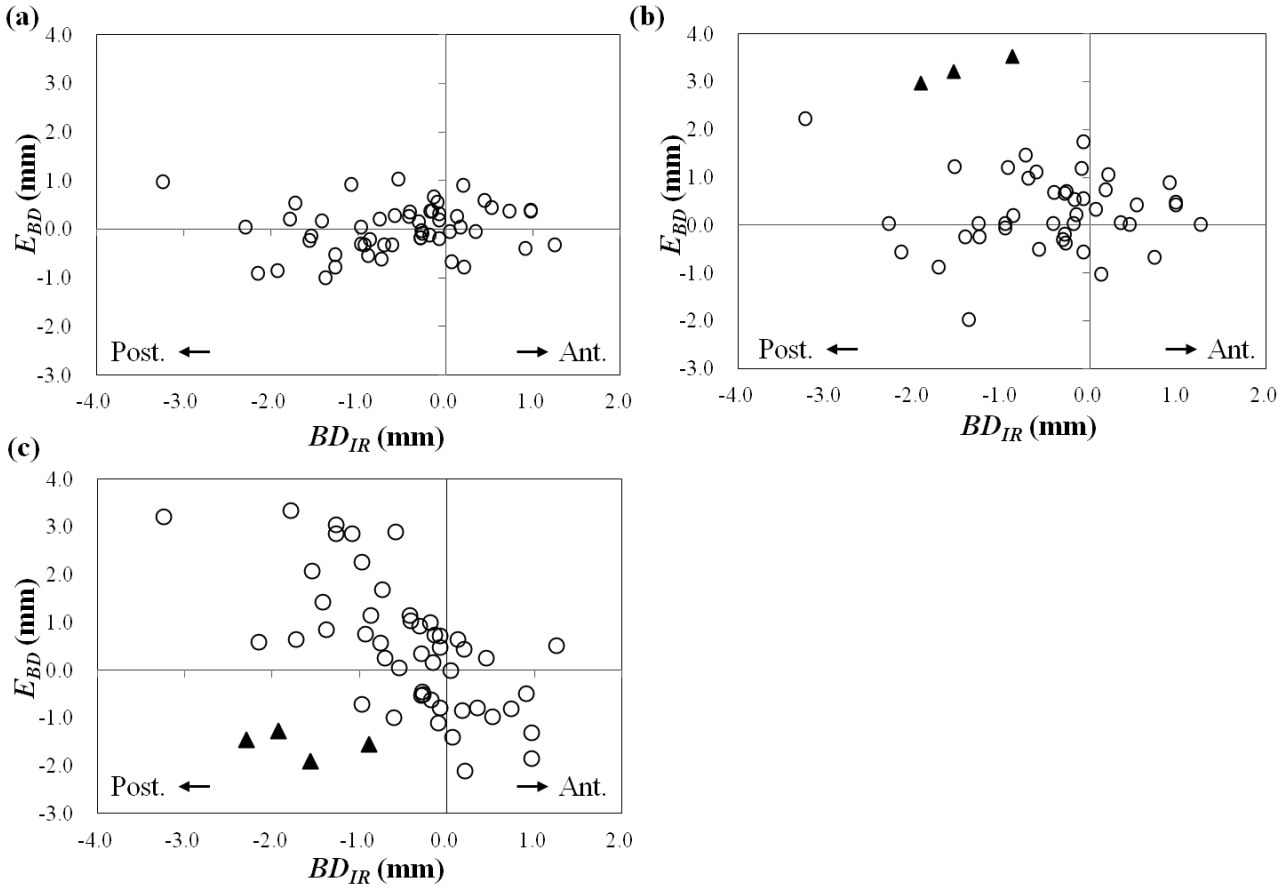

Figure 6. E_{BD} as a function of the baseline drift of the IR marker positions (BD_{IR}) in the (a) LR, (b) AP, and (c) SI directions. $|BD_{detect}|$ > 2 mm in Patient 6 is indicated by triangles.

Figure 7 shows E_{BD} as a function of the elapsed time before updating the 4D model. E_{BD} was distributed randomly rather than systematically. E_{BD} > 3 mm was occasionally observed, even at the median elapsed time.

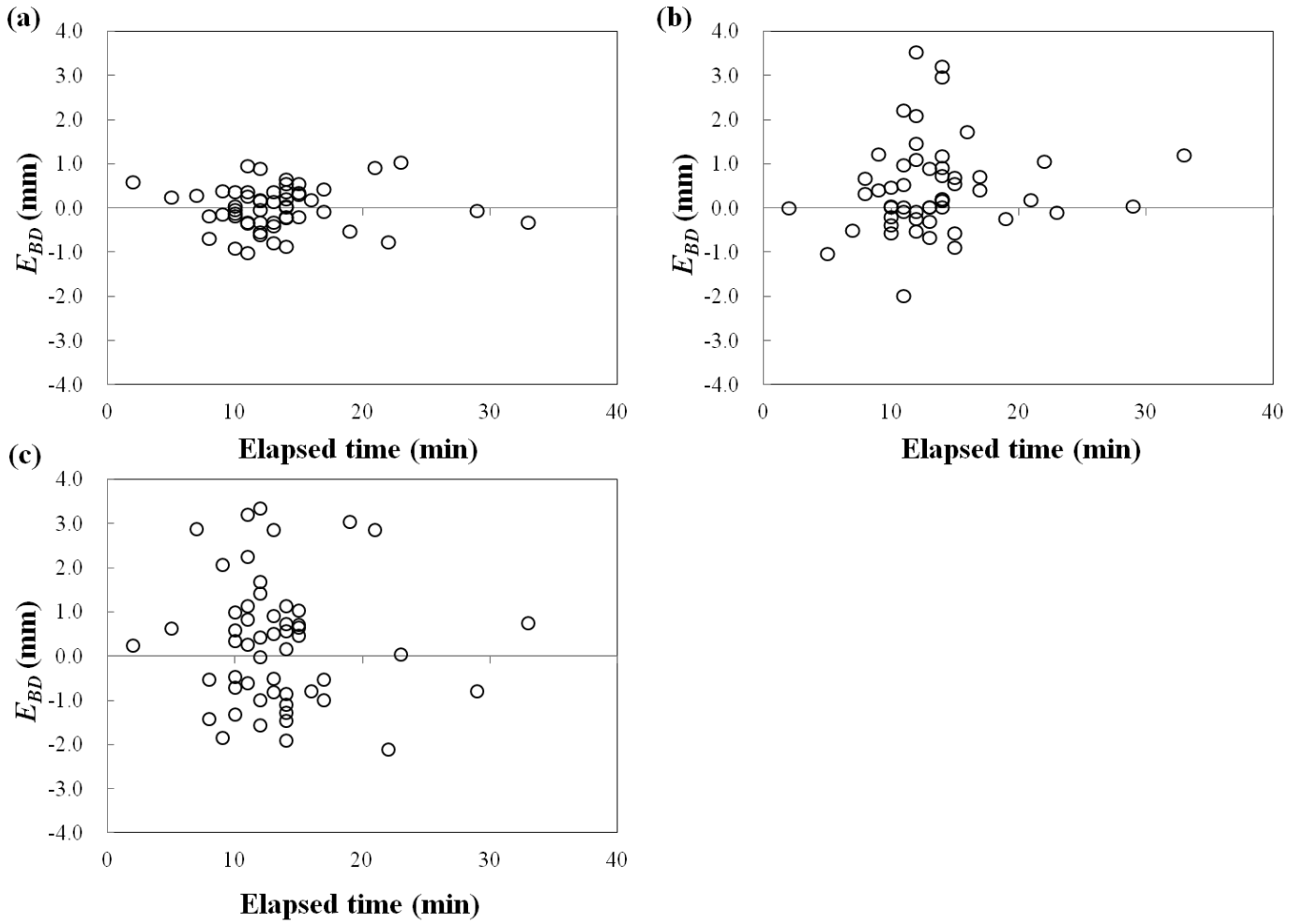

Figure 7. E_{BD} as a function of the elapsed time before updating the 4D model in the (a) LR, (b) AP, and (c) SI directions.

IV. DISCUSSION

We estimated the predictive errors in 4D modeling and those resulting from the baseline drift of the IR marker and detected target positions from logfiles for 10 lung cancer patients who underwent IR Tracking. Our results showed that the Vero4DRT system creates a highly accurate 4D model, although the baseline drift of the IR marker and target positions reduced this accuracy.

Hoogeman *et al*. quantified the clinical accuracy of the Synchrony system, showing that SDs describing intrafraction variations around the whole-fraction mean error were 0.1–1.9 mm for the LR, 0.2–2.5 mm for the AP, and 0.2–1.9 mm for the SI directions.[5] The SD of E_{4DM} was up to 1.6 mm in the current study, which is comparable with their results. In both clinical cases and a phantom study, IR Tracking substantially reduced the geometric error caused by respiratory motion.[11] In the current study, high or moderate correlations between internal target and external IR marker positions were observed for most patients. Meanwhile, small correlations were observed for logfiles of 6.4%, 7.3%, and 1.8% in the LR, AP, and SI directions, respectively. These poor correlations were caused by small motion amplitudes of a target, fluctuations in respiratory signals resulting from heartbeats, and phase shifts between internal target and external IR marker positions. As shown in E_{4DM}, however, the Vero4DRT system was able to compensate for the respiratory motion with high accuracy even under these conditions.

Breathing patterns can vary in magnitude and period during treatment sessions, and expiration baseline drift of the respiratory signals also occurs.[15-17] In general, the cause of baseline drift involves a gradual mechanism, such as muscle relaxation or a change in the method of breathing, and transit events such as deep breathing or a brief

291 halts in breathing.[7,18-21] It is very difficult to manage these events because they occur
292 unconsciously or unexpectedly. Hoogeman *et al*. concluded that the inter- and
293 intrafractional baseline drift altered the correlation between the positions of the internal
294 and external markers.[5] These tendencies were also observed in our study (Figs. 5 and 6).
295 In addition, our data indicated that BD_{IR} was not directly related to BD_{detect}, which was
296 also reported by Malinowski *et al*.,[7] indicating that the 4D model should be updated to
297 correct the relationship between the internal target and external IR marker positions.

298 E_{BD} in the LR and AP directions had a strong correlation with BD_{detect} (Fig. 5).
299 Meanwhile, E_{BD} in the SI direction was caused mainly by BD_{IR}, with the exception of
300 Patient 6 (Fig. 6). The speculated reason for the lack of a correlation between BD_{IR} and
301 E_{BD} in this patient was that abdominal breathing may have switched to chest breathing
302 during a treatment session. When the baselines of the IR marker and target positions
303 systematically deviated from those at the time of 4D modeling during beam delivery, the
304 gimbaled x-ray head would not aim at the actual target position. The best method of
305 avoiding such an unfavorable situation is frequent updating of the 4D model.
306 Malinowski *et al*. reported that the tumor-surrogate relationship mostly changed over a
307 30-min treatment fraction and concluded that such changes must be taken into account
308 for optimal motion management.[7] Our data suggest that it is difficult to determine the
309 optimal timing for 4D model updating because the inter-patient variation in the
310 correlation of E_{BD} with the elapsed time was random (Fig. 7); however, the IR marker
311 and target positions can be monitored during IR Tracking irradiation (Fig. 2). Using this
312 feature, Vero4DRT users should carefully monitor the IR marker and target positions for
313 safe beam delivery and update the 4D model when systematic deviation of these
314 positions is observed.

315 E_{4DM} and E_{BD} are important components in determining the margin size in IR
316 Tracking. In addition, one must consider the interfractional differences in the geometric
317 arrangement between the target and gold markers. Van der Voort van Zyp *et al*.
318 investigated the displacement of 4.0-mm-long platinum markers in 42 lung cancer
319 patients, showing that the displacement of fiducial markers was around 1.0 mm on
320 repeat CT.[22] A similar problem might occur with the implanted gold markers[23]; therefore,
321 the displacement of the implanted gold markers should be considered when determining
322 the overall margin size other than E_{4DM} and E_{BD}.
323
324
325 **V. CONCLUSIONS**
326 We analyzed the predictive errors in 4D modeling and those resulting from
327 baseline drift of the IR marker and target positions for IR Tracking. Application of IR
328 Tracking substantially reduced the geometric error caused by respiratory motion;
329 however, an intrafractional error due to baseline drift of >3 mm was occasionally
330 observed. To compensate for the predictive error resulting from the intrafractional
331 baseline drift, we recommend checking the IR marker and target positions constantly
332 and updating the 4D model several times during a treatment session.

Acknowledgments

This research was supported in part by grants from the Japan Society for the Promotion of Science (JSPS) through the “Funding Program for World-Leading Innovative R&D on Science and Technology (FIRST Program),” sponsored by the Council for Science and Technology Policy (CSTP).

338 **REFERENCES**

339 1. Y. Matsuo, H. Onishi, K. Nakagawa, M. Nakamura, T. Ariji, Y. Kumazaki, M.
340 Shimbo, N. Tohyama, T. Nishio, M. Okumura, H. Shirato, M. Hiraoka, “Guidelines
341 for respiratory motion management in radiation therapy,” J. Radiat. Res. in press
342 (2012).
343 2. P. J. Keall, G. S. Mageras, J. M. Balter, R. S. Emery, K. M. Forster, S. B. Jiang, J.
344 M. Kapatoes, D. A. Low, M. J. Murphy, B. R. Murray, C. R. Ramsey, M. B. van
345 Herk, S. S. Vedam, J. W. Wong, E. Yorke, “The management of respiratory motion
346 in radiation oncology: Report of AAPM Radiation Therapy Committee Task Group
347 No. 76,” Med. Phys. **33**, 3874-3900 (2006).
348 3. S. Dieterich, K. Cleary, W. D’Souza, M. Murphy, K. H. Wong, P. Keall, “Locating
349 and targeting moving tumors with radiation beams,” Med. Phys. **35**, 5684-5694
350 (2008).
351 4. S. Sayeh, J. Wang, W. T. Main, W. Kilby, and C. R. Maurer, “Respiratory motion
352 tracking for robotic radiosurgery,” in *Robotic Radiosurgery: Treating Tumors That*
353 *Move With Respiration*, edited by H. C. Urschel, J. J. Kresl, J. D. Luketich, L.
354 Papiez, and R. D. Timmerman (Springer, Berlin Heidelberg, 2007), pp. 15–29.
355 5. M. Hoogeman, J. B. Prevost, J. Nuyttens, J. Poll, P. Levendag, B. Heijmen,
356 “Clinical accuracy of the respiratory tumor tracking system of the CyberKnife:
357 Assessment by analysis of log files,” Int. J. Radiat. Oncol., Biol., Phys. **74**, 297-303
358 (2009).
359 6. E. W. Pepin, H. Wu, Y. Zhang, B. Lord, “Correlation and prediction uncertainties in
360 the CyberKnife Synchrony respiratory tracking system,” Med. Phys. **38**, 4036-4044
361 (2011).

7. K. Malinowski, T. J. McAvoy, R. George, S. Dietrich, W. D. D'Souza, "Incidence of change in respiration-induced tumor motion and its relationship with respiratory surrogates during individual treatment fractions," Int. J. Radiat. Oncol., Biol., Phys. **82**, 1665–1673 (2012).
8. Y. Kamino, K. Takayama, M. Kokubo, Y. Narita, E. Hirai, N. Kawada, T. Mizowaki, Y. Nagata, T. Nishida, M. Hiraoka, "Development of a four-dimensional image-guided radiotherapy system with a gimbaled X-ray head," Int. J. Radiat. Oncol., Biol., Phys. **66**, 271–278 (2006).
9. Y. Kamino, S. Miura, M. Kokubo, I. Yamashita, E. Hirai, M. Hiraoka, J. Ishikawa, "Development of an ultrasmall C-band linear accelerator guide for a four-dimensional image-guided radiotherapy system with a gimbals x-ray head," Med. Phys. **34**, 1797–1808 (2007).
10. N. Mukumoto, M. Nakamura, A. Sawada, K. Takahashi, Y. Miyabe, K. Takayama, T. Mizowaki, M. Kokubo, M. Hiraoka, "Positional accuracy of novel x-ray-image-based dynamic tumor-tracking irradiation using a gimbaled MV x-ray head of a Vero4DRT (MHI-TM2000)," Med. Phys. **39**, 6287-6296 (2012).
11. N. Mukumoto, M. Nakamura, A. Sawada, Y. Suzuki, K. Takahashi, Y. Miyabe, S. Kaneko, T. Mizowaki, M. Kokubo, M. Hiraoka, "Accuracy verification of infrared marker-based dynamic tumor-tracking irradiation using the gimbaled x-ray head of the Vero4DRT (MHI-TM2000)," Med. Phys. **40**, 041706-1–041706-9(2013).
12. Y. Matsuo, A. Sawada, N. Ueki, Y. Miyabe, M. Nakamura, S. Yano, S. Kaneko, T. Mizowaki, M. Kokubo, M. Hiraoka, "An initial experience of dynamic tumor tracking irradiation with real-time monitoring using Vero4DRT (MHI-TM2000)," Radiother. Oncol. **103**, S64 (2012).

386 13. M. Akimoto, M. Nakamura, N. Mukumoto, M. Yamada, N. Ueki, Y. Matsuo, A.
387 Sawada, T. Mizowaki, M. Kokubo, M. Hiraoka, “Optimization of the x-ray
388 monitoring angle for creating a correlation model between internal and external
389 respiratory signals,” Med. Phys. **39**, 6309-6315 (2012).
390 14. J. Cohen, *Statistical power analysis for the behavioral sciences*, 2nd ed. (Lawrence
391 Erlbaum Associates Inc., Abingdon, 1988).
392 15. S. S. Korreman, T. Juhler-Nottrup, A. L. Boyer, “Respiratory gated beam delivery
393 cannot facilitate margin reduction, unless combined with respiratory correlated
394 image guidance,” Radiother. Oncol. **86**, 61-68 (2008).
395 16. K. J. Redmond, D. Y. Song, J. L. Fox, J. Zhou, C. N. Rosenzweig, E. Ford,
396 “Respiratory motion changes of lung tumors over the course of radiation therapy
397 based on respiration-correlated four-dimensional computed tomography scans,” Int.
398 J. Radiat. Oncol., Biol., Phys. **75**, 1605–1612 (2009).
399 17. B. Zhao, Y. Yang, T. Li, X. Li, D. E. Heron, M. S. Hug, “Statistical analysis of
400 target motion in gated lung stereotactic body radiation therapy,” Phys. Med. Biol.
401 **56**, 1385, (2011).
402 18. C. Ozhasoglu, M. J. Murphy. “Issues in respiratory motion compensation during
403 external-beam radiotherapy,” Int. J. Radiat. Oncol., Biol., Phys. **52**, 1389-1399
404 (2002).
405 19. Y. Tsunashima, T. Sakae, Y. Shioyama, K. Kagei, T. Terunuma, A. Nohtomi, Y.
406 Akine. “Correlation between the respiratory waveform measured using a respiratory
407 sensor and 3D tumor motion in gated radiotherapy,” Int. J. Radiat. Oncol., Biol.,
408 Phys. **60**, 951-958 (2004).
409 20. J. D. P. Hoisak, K. E. Sixel, R. Tirona, P. C. F. Cheung, J-P. Pignol. “Correlation of

410 lung tumor motion with external surrogate indicates of respiration," Int. J. Radiat.
411 Oncol., Biol., Phys. **60**, 1298-1306 (2004).
412 21. D. Ionascu, S. B. Jiang, S. Nishioka, H. Shirato, R. I. Berbeco. "Internal-external
413 correlation investigations of respiratory induced motion of lung tumors," Med. Phys.
414 **34**, 3893-3903 (2007).
415 22. N. C. van der Voort van Zyp, M. S. Hoogeman, S. van de Water, P. C. Levendag, B.
416 van der Holt, B. J. M. Heijmen, J. J. Nuyttens, "Stability of markers used for
417 real-time tumor tracking after percutaneous intrapulmonary placement," Int. J.
418 Radiat. Oncol., Biol., Phys. **81**, e75-e81 (2011).
419 23. M. Imura, K. Yamazaki, H. Shirato, R. Onimura, M. Fujino, S. Shimizu, T. Harada, S.
420 Ogura, H. Dosaka-Akita, K. Miyasaka, and M. Nishimura, "Insertion and fixation of
421 gold markers for setup and tracking of lung tumors in radiotherapy," Int. J. Radiat.
422 Oncol., Biol., Phys. **63**, 1442–1447 (2005).